Real-Time Measurement of Bubbling Phenomena in a Three-Dimensional Gas-Fluidized Bed Using Ultrafast Magnetic Resonance Imaging

C. R. Müller, J. F. Davidson, J. S. Dennis, P. S. Fennell, L. F. Gladden, A. N. Hayhurst, M. D. Mantle, A. C. Rees, and A. J. Sederman

Department of Chemical Engineering, University of Cambridge, Pembroke Street, Cambridge CB2 3RA, United Kingdom

(Received 1 November 2005; published 21 April 2006)

Ultrafast magnetic resonance imaging has been applied for the first time to measure simultaneously both the rise velocities and coalescence of bubbles, and the dynamics of the solid phase in a gas-solid two-phase flow. Here, we consider the hydrodynamics within a gas-fluidized bed of particles of diameter 0.5 mm contained within a column of internal diameter 50 mm; gas velocities in the range of 0.18–0.54 m/s were studied. The data are of sufficient temporal and spatial resolution that bubble size and the evolution of bubble size and velocity following coalescence events are determined.

DOI: 10.1103/PhysRevLett.96.154504 PACS numbers: 47.55.Kf, 45.70.−n, 83.85.Fg

The dynamics of granular systems continue to attract considerable interest in areas such as segregation [1] and, in particular, the fluidlike behavior of granular arrays during flow [2–5] and partially and fully fluidized systems [6–9]. This Letter is concerned with gas-fluidized beds, comprising typically a bed of granular solids supported on a porous plate in a vertical column, through which a gas flows upwards. The solids become fluidized when the flow rate of gas is large enough for the pressure drop across the bed to become equal to the weight of the bed per unit area of the column. The superficial velocity of the gas, defined as volumetric flow rate divided by the cross-sectional area of the column, required to just fluidize the bed is U_{mf}. Gas in excess of that required for this minimum fluidization generally forms bubbles. Here, we demonstrate the use of MRI techniques to probe and quantify the fundamental granular dynamics of these systems. The motivation for this study is that various hydrodynamic phenomena in fluidized beds, e.g., the coalescence and formation of bubbles, are still not well understood, primarily because it has been difficult to observe the motion of opaque solids and bubbles far from the influence of the walls of the containing vessel. For example, the development and validation of theories of bubble coalescence have so far been restricted to using observations recorded in so-called 2D fluidized beds [10], which are rectangular units with two vertical transparent parallel walls close together (e.g., 5–20 mm), so that bubbles bridge the gap between them; such an arrangement cannot be free from the influence of the walls. Indeed, even the theoretical models of the rise velocity of bubbles in a fluidized bed are equivocal: it is unclear whether or not the superficial velocity of the gas above that required for fluidization, $U - U_{\mathrm{mf}}$, should be added to the velocity of rise of a single bubble in a fluidized bed at minimum fluidization. Previous attempts to study 3D fluidized beds experimentally have included simple capacitance or optical probes [11], x-ray photography [12], or more recently capacitance tomography [13], diffusive-wave spectroscopy [14], and magnetic resonance (MR) [8,9,15–17]. Of these, MR offers a unique capability to image the dynamics of the bed in real time with sufficient spatial resolution to determine the movement of individual bubbles. To date, MR has been applied to fluidized bed systems in two distinct ways; imaging either the solid or the gas phase. The initial work on solid-phase measurements was reported by Savelsberg *et al.* [9] who employed time averaged **k**-space and **q**-space MR methods to monitor time averaged density variations and the rms displacement of particles. These measurements were made on the entire granular ensemble, so the results represented the statistically averaged behavior of the whole system. More recently, MRI of the solid phase has been applied to image mixing and dispersion of solids introduced into a fluidized bed [15], to provide 2D maps of solids velocity [16,17] and to image jet formation and structure at the point of gas injection into the granular array [17]. Imaging of the gas phase directly is less well studied. To date, the only application of such an approach is the use of laser-polarized ^{129}Xe to measure gas exchange between bubble and emulsion phase and the gas velocity distribution within the bed [8]. In this Letter, we report the first use of ultrafast MRI to record the distribution of solids along the length of the bed in real time. Interfaces between gas and solid are identified and tracked with sufficient time resolution (1.34–2.08 ms) and spatial resolution (1.25–0.625 mm) that the dimension of gas bubbles and gas rise velocities are quantified. Further, bubble coalescence events are imaged. The fluidized bed used was contained in a Perspex column (i.d. 50 mm, total length 1.8 m), fitted with a perforated plate (Perspex) distributor containing 37 holes, each of 1.0 mm diameter. The bed was fluidized with nitrogen, which was humidified to eliminate electrostatic effects. The fluidized particles were naturally oil-containing nudicaule seeds with a mean diameter $d_p =$ 0.5 mm. In the MRI experiment, the signal is obtained from the oil within the seed, an approach well established

in studying granular flows with MRI [18]. Hence, the distribution of solids within the bed is imaged directly. No MR signal is obtained from the gas.

MRI techniques are based on the ability to encode spatial information in the MR signal. In a spatially unresolved experiment, the sample of interest is placed in a superconducting magnetic field, B_0. Under these conditions, the Larmor precession frequency, ω, of a spin species of gyromagnetic ratio γ is given by $\omega = \gamma B_0$. If, in addition to the large static magnetic field, B_0, a smaller magnetic field, G_z, is applied along the axial (z) direction, the strength of which varies linearly in space, the Larmor precession frequency of the spins now depends linearly on their position along the direction of the applied gradient G_z, viz, $\omega(z) = \gamma(B_0 + G_z z)$. The Fourier transform of the acquired MR signal then yields the one-dimensional (1D) distribution, or profile, of spin densities within the sample. The 1D profile is a quantitative measurement of the solids distribution along the length of the bed. Data were acquired using a Bruker DMX 200 spectrometer, operating at a proton (^{1}H) frequency of 199.7 MHz, equipped with a birdcage radio frequency (rf) coil of length and internal diameter 64 mm. Spatial resolution was achieved using a shielded gradient system capable of producing a maximum magnetic field gradient of 0.139 T/m. A standard 1D FLASH sequence [19], using pulsed magnetic field gradients with gradient echo acquisition, was used with a single excitation pulse, to produce profiles of the distribution of solids, I_z, along the length of the bed. The data are acquired such that the signal intensity at a given height z represents the integral of the signal intensity associated with all solid particles present within the transverse section of the bed at that position. Low (1.25 mm) and high (0.625 mm) spatial resolution 1D profiles were acquired with data acquisition times of 384 and 853 μs, respectively. In a given experiment 8192 independent 1D profiles were acquired at time intervals of 1.34 and 2.08 ms, respectively.

Figure 1 shows high spatial resolution MRI measurements recorded near the top of the fluidized bed: white areas represent a high density of seeds, viz, particulate phase, whereas black represents voids, viz, a bubble or slug. Here, ''slug'' refers to a gas bubble whose diameter is comparable to that of the containing column. Figure 1(a) shows two well-defined slopes, identifying two distinct rise velocities within the bed: (i) the lower slope is a measure of the rise velocity of the particulate phase, in this case the gas-solid interface defines the upper surface of the bed, and (ii) the steeper slope gives the rise velocity of an erupting slug just below the top of the bed (i.e., the movement of a gas-solid interface within the bed is tracked). The signal intensity associated with a slug appears as gray (as opposed to zero intensity, black) because particles rain down at the wall of the column as the slug passes. As seen from Figs. 1(a) and 1(b) slugs may be longer than the length

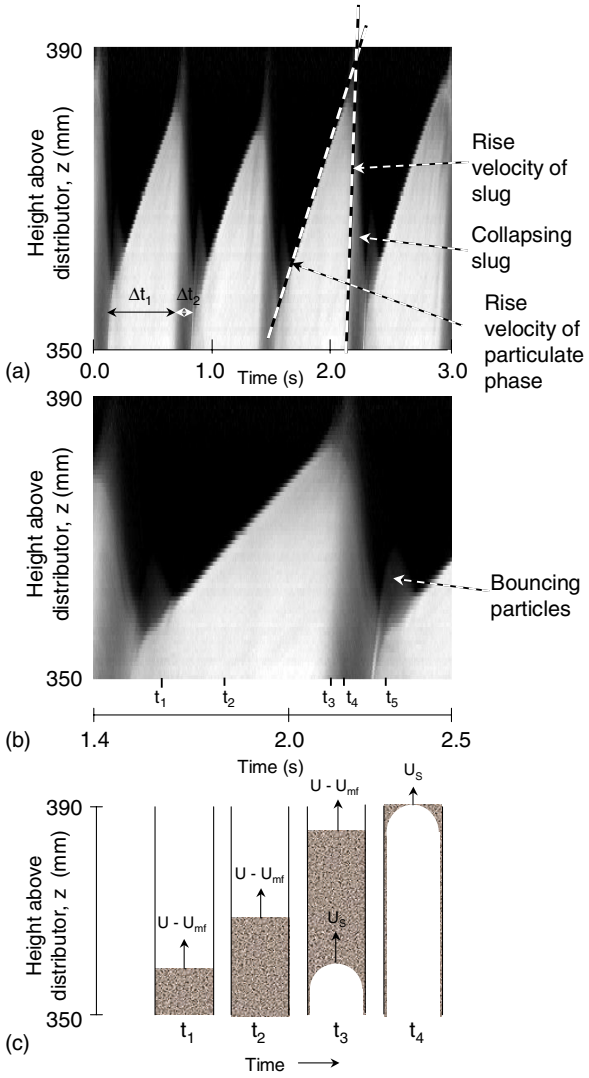

FIG. 1 (color online). (a) Time-resolved MR intensity profiles, I_z, within a nitrogen-fluidized bed of $d_p = 0.5$ mm particles. Unfluidized height 322 mm, $U - U_{mf} = 0.048$ m/s (b) Expanded section of (a) showing in detail the features in the MRI data as a gas slug moves in the field of view and breaks through the top surface of the bed. (c) Schematic of the gas-solid distribution within the bed at times t_1, t_2, t_3, t_4 identified in (b).

of the imaging region (40 mm). After eruption of the slug, the falling particles are seen to bounce on the top of the bed, as identified in Fig. 1(b). The respective times, Δt_1 and Δt_2, taken for a plug of solids and the following slug to pass a given height can be measured as shown in Fig. 1(a), in this case at $z = 355$ mm above the distributor. Figure 1(b) shows a section of Fig. 1(a) with the time axis expanded in the range 1.4–2.5 s. Figure 1(c) shows a schematic of the structure of the bed at times t_1–t_4, identified in Fig. 1(b), during one cycle of slug breakthrough at the surface of the bed. At times t_1 and t_2 only particulate phase and free space above the bed are present in the field of view. The upper surface of the bed is clearly

defined by the interface between the black and white pixels. At time t_3, a slug has entered the imaging region; this slug reaches the top of the bed at time t_4. After eruption of the slug at time t_4, the surface of the bed collapses. The remaining particles associated with the slug fall down adjacent to the walls of the bed. These particles are manifested by the dark-gray area to the right of the t_4 line. After the slug has collapsed, a new top surface of the bed is formed, indicated by the clear change in slope at t_5 in Fig. 1(b). The negative slope of the gray-black boundary for $t_4 < t < t_5$ indicates the fall of the residual particles at the wall during the collapse of the slug. Confirmation that our interpretation of these data is correct was achieved as follows. From MRI data, the rise velocity of the particulate phase at the top was calculated as 0.043 ± 0.003 m/s, which compares well with $U - U_{\mathrm{mf}} = 0.048 \pm 0.005$ m/s, the results confirm that the velocity of the upper surface equals the excess gas velocity ($U - U_{\mathrm{mf}}$), in agreement with the two-phase theory of fluidization [20].

Closer to the distributor smaller regions of gas can be imaged. Figure 2 shows typical results, the quality of the data being sufficient for the dimensions of individual bubbles, in the axial direction, to be measured. More importantly, these data enable us to follow bubble coalescence in real time. Consider Fig. 2 in the time intervals 1.4–2.1 s and 2.5–3.0 s; in each case two individual bubbles are seen to merge. The signal intensity at a given position will depend on the dimension of the bubble in the transverse plane. From the data shown in Fig. 2 it is also possible to track the position of the upper gas-solid interface within the bed and hence quantify the rise velocity of the bubble(s) pre- and post-coalescence. In Fig. 2, deceleration of the gas bubbles within the bed is observed upon coalescence, identified by a decrease in the slope of the gas-solid interface, followed by acceleration post-coalescence. This acceleration of the merged bubble and its change in dimensions during coalescence is in qualitative agreement with visual observations made in 2D beds [10].

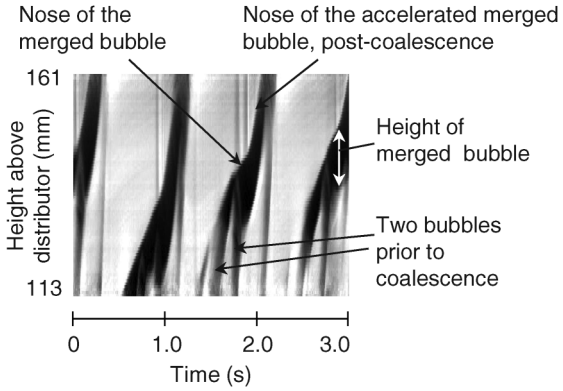

FIG. 2. MR image of the coalescence of bubbles, $U - U_{\mathrm{mf}} = 0.075$ m/s, $U/U_{\mathrm{mf}} = 1.6$.

Figure 3 shows the rise velocity of bubbles and slugs in a fluidized bed as a function of height above the distributor. The rise velocity is obtained by cross-correlating two MRI signals I_1 and I_2 separated by a small vertical distance (7.5 mm), i.e., $R_{12}(\tau) = \lim_{T\to\infty} \frac{1}{T} \int_0^{+T} I_1(t) I_2(t+\tau) dt$. The first maximum of the cross-correlation function, R_{12}, gives the time shift of the MRI signal. Since both the time shift and the vertical distance between the two MR signals are known, the velocity of the bubble or slug can be calculated. The average of two cross-correlation analyses (of high time resolution MR data, similar to that shown in Fig. 2 and extending over an acquisition time of ~11 s) gave the values plotted in Fig. 3. Figure 3 can be divided into three sections: (i) Below a height, h, above the distributor of 100 mm, the bubble rise velocity fluctuates consistent with the occurrence of bubble coalescence events. (ii) The midsection, $100 < h < 175$ mm, is identified by a relatively constant bubble rise velocity suggesting fewer coalescence events. This section is probably a transition region between bubbling and slugging, where the bubble diameter is becoming comparable to that of the column, but the slugs are not yet fully developed. (iii) In the top section, $h > 175$ mm, a sharp increase in gas rise velocity is seen. At these heights, the axial profiles of solids distribution indicate the transition from bubble to slug flow has occurred. The rather noisy behavior of the rise velocity in this region of the bed is consistent with visual observations of the nonuniform rise velocities of slugs.

Figure 3 also shows published correlations predicting the rise velocities of bubbles and slugs for comparison with the direct MR determination. Consider first the region of the bed up to a height of 175 mm above the distributor. Four correlations for the rise velocity U_B, of a single bubble are plotted in this region. The first two of these are those of Davies and Taylor [21], $U_B = 0.71\sqrt{gD_e}$, and Wallis [22], $U_B = 0.71\sqrt{gD_e} \times 1.13 \exp(-D_e/D_t)$ for $0.125 < D_e/D_t < 0.6$ and $U_B = 0.71\sqrt{gD_e} \times 0.496(D_e/D_t)^{-0.5}$ for $D_e/D_t > 0.6$, where D_e and D_t are

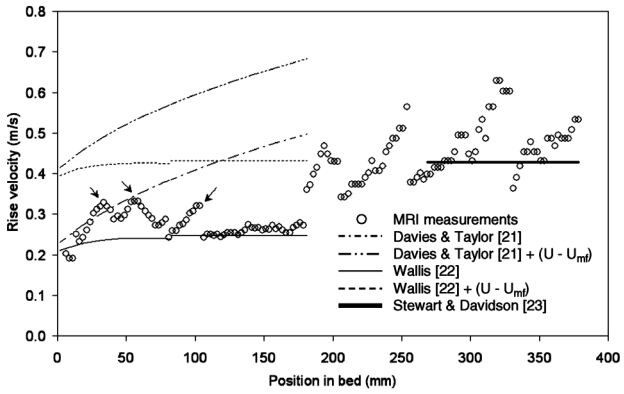

FIG. 3. Rise velocity of bubbles and slugs, $U - U_{\mathrm{mf}} = 0.185$ m/s, $U/U_{\mathrm{mf}} = 2.64$. Arrows indicate positions at which there exists a higher probability of bubble coalescence events.

the diameters of a bubble and the bed, respectively. The expression of Davies and Taylor [21] is derived from a simple analysis based on potential flow theory. The correlation of Wallis [22] is a version of the correlation of Davies and Taylor [21] modified to account for wall effects. The two additional correlations add the term $(U - U_{\mathrm{mf}})$ to the equations of Davies and Taylor [21], and Wallis [22]. This follows from the observation that for slug flow, the rise velocity of a slug is given by $U_S = 0.35\sqrt{gD_t} + (U - U_{\mathrm{mf}})$ [23], where $0.35\sqrt{gD_t}$ is the rise velocity of a slug in an incipiently fluidized bed. Some authors have assumed that the same applies for bubbles, e.g., Ref. [24]. In these correlations a value of the equivalent diameter, D_e of the bubble is required. Since only a determination of bubble height has been obtained from these data, the correlation of Darton *et al.* [25] was used to estimate D_e, viz, $D_e = 0.54(U - U_{\mathrm{mf}})^{0.4}(h + 4\sqrt{A_0})^{0.8}g^{-0.2}$, where A_0 is the area of the distributor divided by the number of holes. Figure 3 clearly shows that, for $h < 175$ mm, the analysis of Wallis [22] provides the best agreement with the MR data, and that the additional term $(U - U_{\mathrm{mf}})$ is not required. Consider now the rise velocity at heights greater than 175 mm, where slug flow prevails. The MR data are compared with the correlation of Stewart and Davidson [23] for slug velocity, viz, $U_S = (U - U_{\mathrm{mf}}) + 0.35\sqrt{gD_t}$, based on potential flow theory and with the $U - U_{\mathrm{mf}}$ term introduced by continuity; the MR results are in excellent agreement with this correlation.

For completeness and to assess the robustness of our conclusions based on the value for D_e used in the correlations a comparison of the predictions of Darton *et al.*'s [25] correlation with the bubble heights measured by MRI was performed. To estimate D_e from the MRI measurements of bubble height, it was necessary to assume a bubble wake angle; this was chosen to be 120° which is typical for bubbles in fluidized beds of the solids used in this study (Geldart's classification B) [24]. At $h = 104$ mm and $U - U_{\mathrm{mf}} = 0.130$ m/s, Darton *et al.*'s [25] correlation predicts $D_e = 30.2$ mm compared to values of 31.5–38.6 mm deduced from the MRI data. If a wake angle of 180°, appropriate to the case of spherical bubbles, is assumed, values of D_e lie in the range of 25.0–30.6 mm. The similar values of D_e obtained from the correlation of Darton *et al.* [25] and from the MRI data give strong support to our interpretation of the MRI intensity profiles in terms of the axial dimension of bubbles within the bed. Further, and more importantly, our conclusions regarding the agreement of the correlations identified in Fig. 3 with the MR data are robust to the values of D_e used regardless of whether they are taken from Darton *et al.*'s [25] correlation or estimates from the MR data, assuming either of the two different wake angles.

In conclusion, MRI has been used for the first time to quantify, simultaneously, gas and solids rise velocities within a 3D fluidized bed. The spatial and temporal resolution is sufficient to follow individual gas bubbles and bubble coalescence events in real time. No signal averaging is employed in these measurements. Hence, this work represents the first report of the imaging of the dynamics of granular flows at ~1 ms time resolution. Preliminary comparison of the MR data with existing correlations, confirm that the rise velocity of the gas phase only requires a term for the excess gas velocity $(U - U_{\mathrm{mf}})$ when slug flow is established. These data will also enable a detailed critical evaluation of the performance of numerical codes in predicting the behavior of 3D gas-fluidized granular arrays.

[1] S. R. Dahl and C. M. Hrenya, Phys. Fluids **16**, 1 (2004).
[2] S. L. Conway, T. Shinbrot, and B. J. Glasser, Nature (London) **431**, 433 (2004).
[3] L. E. Silbert, Phys. Rev. Lett. **94**, 098002 (2005).
[4] O. Pouliquen, Phys. Rev. Lett. **93**, 248001 (2004).
[5] E. E. Ehrichs *et al.*, Science **267**, 1632 (1995).
[6] D. Volfson, L. S. Tsimring, and I. S. Aranson, Phys. Rev. Lett. **90**, 254301 (2003).
[7] C. Huan *et al.*, Phys. Rev. E **69**, 041302 (2004).
[8] R. Wang *et al.*, Magn. Reson. Imaging **23**, 203 (2005).
[9] R. Savelsberg *et al.*, Phys. Rev. E **65**, 020301 (2002).
[10] S. P. Sit and J. R. Grace, Chem. Eng. Sci. **36**, 327 (1981).
[11] D. Harrison and L. S. Leung, Trans. Inst. Chem. Eng. **39**, 409 (1961).
[12] P. N. Rowe and C. X. R. Yocono, Chem. Eng. Sci. **31**, 1179 (1976).
[13] Y. T. Makkawi and P. C. Wright, Chem. Eng. Sci. **57**, 2411 (2002).
[14] N. Menon and D. J. Durian, Science **275**, 1920 (1997).
[15] P. S. Fennell *et al.*, Chem. Eng. Sci. **60**, 2085 (2005).
[16] S. Harms, S. Stapf, and B. Blümich, J. Magn. Reson. **178**, 308 (2006).
[17] A. C. Rees *et al.*, Chem. Eng. Sci. (to be published).
[18] M. Nakagawa *et al.*, Exp. Fluids **16**, 54 (1993).
[19] A. Haase *et al.*, J. Magn. Reson. **67**, 258 (1986).
[20] R. D. Toomey and H. F. Johnstone, Chem. Eng. Prog. **48**, 220 (1952).
[21] R. M. Davies and G. Taylor, Proc. R. Soc. A **200**, 375 (1950).
[22] G. B. Wallis, *One-dimensional Two-Phase Flow* (McGraw-Hill, New York, 1969).
[23] P. S. B. Stewart and J. F. Davidson, Powder Technol. **1**, 61 (1967).
[24] D. Kunii and O. Levenspiel, *Fluidization Engineering* (Butterworth-Heinemann, Stoneham, USA, 1991).
[25] R. C. Darton *et al.*, Trans. Inst. Chem. Eng. **55**, 274 (1977).